LETTER TO THE EDITOR

Rational design and crystallographic analysis of novel isoform-selective TRKA inhibitors for cancer therapy

KEY WORDS

Cancer therapy;
Co-crystal structure;
Drug discovery;
Selective inhibitor;
TRKA

To the Editor:

Tropomyosin receptor kinase A/B/C (TRKA/B/C) are encoded by neurotrophic tyrosine receptor kinase 1/2/3 (NTRK1/2/3), respectively. NTRK gene fusions are the most common drivers of malignancies. Additionally, TRKA is the most common oncogene in TRK family, which is detected in 7.4% of human tumors, and TRKB/C rank 0.4%/3.4%, respectively[1]. Therefore, inhibition of the activated TRKA is an effective anti-tumor approach. Previously discovered Larotrectinib (LOXO-101), Entrectinib (RXDX-101), compounds **7b** and **8** for NTRK-fusion tumors are pan-TRK inhibitors without subtype selectivity (Supporting Information Fig. S1A), causing a series of side effects[2−4]. So far, there have been no reports of TRKA selective inhibitors for clinical anti-tumor therapy or clinical trials, and no related studies have been published. Herein, based on computer-aided drug design and guided compound synthesis, we discovered a TRKA selective inhibitor **32h** (TRKA, IC$_{50}$ = 72 nmol/L; TRKB/C, IC$_{50}$ > 1000 nmol/L). Importantly, compared with broad-spectrum TRKs inhibitors, **32h** exerts anti-tumor effect by selectively inhibiting TRKA to regulate Hippo-YAP and Wnt pathways. The highlights of the study are outlined as follows:

1. Design and synthesis of isoform-selective TRKA inhibitors

The amino acid residues of TRKA were 72%−75% identical to those of TRKB/C in kinase domain[5]. In the membrane-proximal region at amino acid residues 440−497, the homology between TRKA and TRKB/C was greatly reduced by 36%−40% (Fig. S1B). Therefore, it is feasible to design selective TRKA type-II kinase inhibitors that can interact with the near-membrane region. Based on the reported interactions between TRKA and small molecule inhibitors, Met592, Phe589 and Phe669 were key to TRKA activity. Moreover, three-dimensional quantitative structure−activity relationships (3D-QSAR) and pharmacophore characteristics of TRKA were obtained (Fig. 1A). Next, compound **8** was discovered by multiple docking, which could serve as a lead for further drug design and structural modification (Fig. 1B and Fig. S1C−E).

Subsequently, various substituted benzene rings were introduced into the terminal of **8** to occupy the hydrophobic cavity, then compounds **16a−aa**, **19a−c**, **21a−b** and **23a−c** were acquired, respectively. Among them, **16w** exhibited an excellent TRKA inhibitory rate of 80.33% at 1 μmol/L, and remarkable isoform selectivity with inhibitory rates of 11.64%/4.59% against TRKB/C, respectively. Therefore, the best TRKA kinase selectivity and anti-proliferative activities were achieved in compounds with the linker ureido (Fig. S1F−G, Supporting Information Tables S1 and S2). Based on this, **26a−k** were synthesized and **26h** presented the best inhibitory rate and selectivity against TRKA (87.67%) with IC$_{50}$ value of 5.52 μmol/L in KM12-Luc (TPM3-NTRK1) cells of colorectal cancer (CRC) (Supporting Information Table S3). The overlaying of docking pattern of **26h** and **16w** with TRKA showed that the modification of central benzene ring caused the displacement of core group 1*H*-indazole to hinge region (Fig. S1H−I). To increase the interaction with

---

TRKA hinge region, a variety of substituted groups were introduced at the 3-position of 1*H*-indazole. Significantly, methylpyrazole (**32b−d**, **32f** and **32h**) all enhanced inhibitory activity to TRKA and inhibitory effect against KM12-Luc cells. Collectively, through structural optimization of hydrophobic region, linker, central benzene ring and hinge region, **32h** exhibited the most potent kinase inhibitory (TRKA IC$_{50}$ = 72 nmol/L) and antiproliferative (IC$_{50}$ = 1.62 μmol/L) activities (Supporting Information Table S4 and Fig. 1C and Fig. S1J).

2. The co-crystal structure and molecular dynamics (MD) simulation of TRKA−32h complex

To explore the binding mode of **32h** with TRKA, we solved the crystal structure of the TRKA/**32h** complex (PDB code 7XBI) at 2.16 Å resolution, in which **32h** binds to the DFG-out/αC-helix-out conformation of TRKA (Fig. 1D and Supporting Information Table S5). As shown, the 1*H*-indazole group of **32h** formed two hydrogen bonds with Glu590 and Met592, and amide groups formed a hydrogen bond with the adjacent water molecule. Besides, the ureido of **32h** formed hydrogen bonds with Glu560 on the αC-helix and Asp668 on the DFG loop, respectively. We also found that its trifluoromethyl group made face-to-edge π−π stacking and hydrophobic interactions with Phe589 and Phe669, where the F atom of trifluoromethyl group formed a weak hydrogen bond with Lys544. Moreover, the substituted phenyl group of **32h** extended into the hydrophobic pocket composed of Leu563, Leu564, Leu567, Ile572, Val573, Ile666, Leu641, Phe646 and His648, and was further stabilized through hydrophobic contacts.

Based on the crystal structure of TRKA−32h complex, we further used MD simulation to investigate the dynamic binding mode. By calculating the root mean square deviation (RMSD) and binding free energy, and analyzing the superposition of three complexes, it was found that the selectivity of 32h binding to TRKA was mainly attributed to the large difference between arginine and phenylalanine (Fig. S1K−M, Fig. 1E and Supporting Information Table S6). Notably, **32h** had a lower RMSF in TRKA−32h complex, suggesting that it fluctuate less and bind more stably (Fig. 1F). And the distance between the side chain benzene ring center of TRKA-Phe669 and the middle benzene ring of **32h** is small, which can form an edge-face stacked interaction, while TRKB-Phe711 and TRKC−Phe698 cannot form such interaction (Fig. 1G).

3. Kinase selectivity analysis of 32h

Among tyrosine kinases, **32h** presented the best inhibitory effect on TRKA (Fig. 1H). Moreover, it also possessed over 60% inhibition rate for eight kinases including PRKG2 (Supporting Information Tables S7 and S8). To further analyze the selectivity and efficacy of **32h**, CRC cell line HCT116 with a higher affinity was used to construct those with NTRK overexpression and gene fusion. Given that TRKs overexpression and gene fusion share the same kinase domain, HCT116 cells overexpressing NTRK 1/2/3 (NTRK1/2/3-OE) and harboring ETV6-NTRK1/2/3 fusion gene (ETV6-NTRK1/2/3-OE) were constructed. As expected, **32h** dose-dependently downregulated p-TRKA, but not p-TRKB/C (Fig. 1I), and it exerted the inhibitory effect on CRC cells *via* downregulating TRKA and downstream ERK1/2, AKT and PLCγ (Fig. 1J).

4. Anti-tumor effect and molecular mechanism of 32h

To clarify the molecular mechanism, RNA sequencing was performed in NTRK1-OE HCT116 cells treated with **32h**. Volcano plot exhibited all up- and down-regulated differentially expressed genes (DEGs), KEGG analysis revealed significant enrichment of Hippo signaling pathway, and cluster heatmap showed marked downregulation of Wnt5a, IGFBP5, CX3CR1 and CXCL10 (Fig. 1K−M). Since Hippo/YAP and Wnt/β-Catenin pathways are involved in the carcinogenesis of CRC, we thereafter examined their key proteins in cells, indicating that **32h** dose-dependently downregulated YAP in Hippo pathway, and Wnt5a and β-Catenin in Wnt pathway (Fig. 1N). Additionally, both **32h** and pan-TRK inhibitor RXDX-101 significantly downregulated these proteins in HCT116 or NTRK1-OE cells, especially in the latter (Fig. 1O). A previous study has shown that Hippo pathway can mediate Wnt pathway, so we considered that **32h** exerted anti-tumor role in CRC by inactivating Hippo and Wnt pathways *via* inhibiting TRKA.

Since Wnt/β-catenin pathway negatively regulates autophagy, we next explored the involvement of autophagy in **32h**-induced NTRK1-OE cell death. Apparently, **32h** could induce autophagy, simultaneously up-regulate p62 and LC3II, and decrease cell viability (IC$_{50}$ = 5.2 μmol/L). To clarify whether the **32h**-induced autophagy is protective or lethal to cells, the addition of autophagy inhibitors chloroquine (CQ) and bafilomycin A1 (Baf-A1) revealed that it not only inhibited the late autophagy, but also enhanced LC3II accumulation and cell death (Fig. 1P−T), indicating that **32h** induced autophagy but inhibited autophagic flux, eventually causing cell rupture and death due to abnormal accumulation of autophagosomes. Accordingly, **32h** markedly inhibited the colony formation and blocked the cell cycle from G0/G1 to S phase, and different apoptosis experiments consistently identified increased apoptosis (Fig. 1U−Y). Subsequently, **32h** was injected into Sprague−Dawley (SD) rats *via* tail vein, and found to possess good pharmacokinetic properties and plasma concentration (Fig. S1N and Supporting Information Table S9). Based on good anti-tumor effect and pharmacokinetic properties of **32h**, the *in vivo* efficacy was further evaluated in xenograft models. The tumor volumes and weights of treatment groups were noticeably lower than those of model groups, and hematoxylin-eosin (H&E) staining of tissues did not visualize significant pathological changes, suggesting the safety of **32h** (Supporting Information Fig. S2).

In conclusion, we discovered a highly selective TRKA inhibitor **32h** with an IC$_{50}$ of 72 nmol/L for TRKA but greater than 1000 nmol/L for TRKB/C. Additionally, kinomics and co-crystallization experiments together reflect its targeting and high selectivity, and different from pan-TRKs inhibitors, RNA-seq analysis indicates that **32h** exerts anti-tumor effects by selectively inhibiting TRKA to modulate Hippo-YAP and Wnt pathways. Importantly, its good pharmacokinetic properties and anti-tumor efficacy *in vivo* xenograft models also suggest that TRKA selective inhibitors could be used as a therapeutic strategy for NTRK1 fusion-positive cancers.
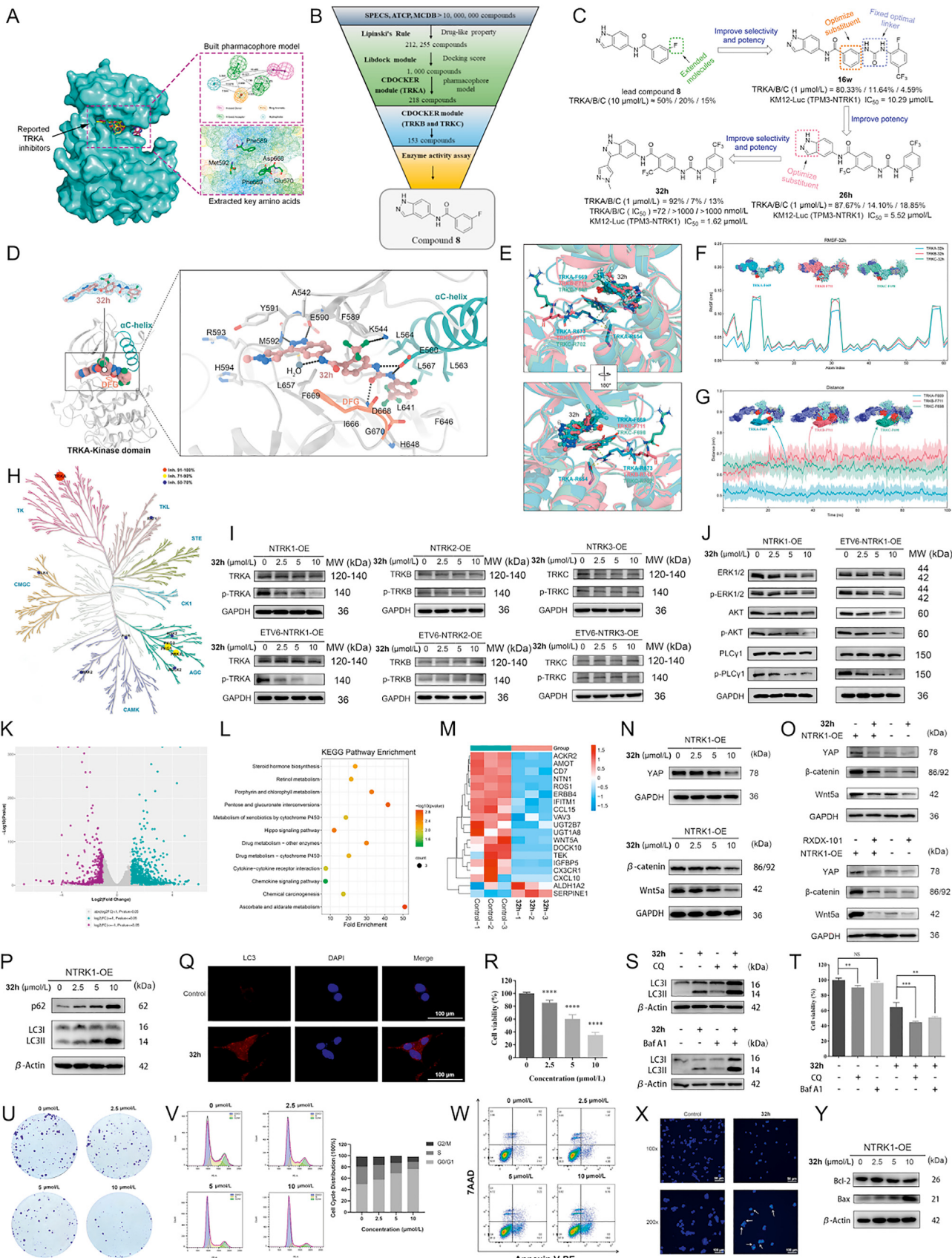
Acknowledgments

Author contributions

Liang Ouyang and Qiu Sun conceived and oversaw the project. Guan Wang designed the synthetic routes and biological experiments. Yongya Wu performed the biological assays, analyzed the data and wrote the manuscript. Chengyong Wu participated in crystal analysis and molecular dynamics simulation. Guan Wang and Tingting Jiang completed the synthesis and wrote the first manuscript. Wen Shuai, Aoxue Wang and Faqian Bu assisted the chemical synthesis.

Conflicts of interest

The authors declare no conflicts of interest.

Appendix A.   Supporting information

Supporting data to this article can be found online at https://doi.org/10.1016/j.apsb.2022.10.012.

References

1. Yan W, Lakkaniga NR, Carlomagno F, Santoro M, McDonald NQ, Lv F, et al. Insights into current tropomyosin receptor kinase (TRK) inhibitors: development and clinical application. *J Med Chem* 2019;**62**:1731−60.
2. Drilon A. TRK inhibitors in TRK fusion-positive cancers. *Ann Oncol* 2019;**30**:viii23−30.
3. Wang Z, Wang J, Wang Y, Xiang S, Song X, Tu Z, et al. Discovery of the first highly selective and broadly effective macrocycle-based type II TRK inhibitors that overcome clinically acquired resistance. *J Med Chem* 2022;**65**:6325−37.
4. Zhuo L, Wang M, Wu F, Xu H, Gong Y, Yu Z, et al. Discovery of next-generation tropomyosin receptor kinase inhibitors for combating multiple resistance associated with protein mutation. *J Med Chem* 2021;**64**:15503−14.
5. Zhang L, Zhang L, Guo Y, Xiao M, Feng L, Yang C, et al. MCDB: a comprehensive curated mitotic catastrophe database for retrieval, protein sequence alignment, and target prediction. *Acta Pharm Sin B* 2021;**10**:3092−104.

Guan Wang[†], Yongya Wu[†], Chengyong Wu[†], Wen Shuai, Tingting Jiang, Aoxue Wang, Faqian Bu, Qiu Sun[*], Liang Ouyang[*],

State Key Laboratory of Biotherapy and Cancer Center, Innovation Center of Nursing Research, Nursing Key Laboratory of Sichuan Province, National Clinical Research Center for Geriatrics, West China Hospital, and Collaborative Innovation Center of Biotherapy, Sichuan University, Chengdu 610041, China

*Corresponding authors.
E-mail addresses:* sunqiu@scu.edu.cn (Qiu Sun),
ouyangliang@scu.edu.cn (Liang Ouyang)

[†]These authors made equal contributions to this work.

Figure 1 Discovery and anti-tumor studies of selective TRKA inhibitors. (A) Establishment of TRKA small molecule pharmacophores and extraction of key amino acids. (B) Virtual screening process. (C) The structure−activity relationship evolution from lead **8**−**32h**. (D) X-ray co-crystal structure of **32h**. (E) Superposition of active sites of TRKA−**32h** (blue), TRKB−**32h** (red), and TRKC−**32h** (green) complexes. (F) RMSF at **32h** in different complexes. (G) Distances between the center of the phenylalanine side chain near the TRKs active site and the center of **32h** intermediate phenyl ring. (H) Kinase selectivity profile. (I−J) Effects of **32h** on TRKs phosphorylated proteins and downstream pathways of NTRK overexpressing and fusion cells. (K) Volcano plot showing DEGs (blue for up-regulation, purple for down-regulation, and grey for no significant change). (L) Representative KEGG pathway analysis. (M) Cluster heatmap. (N) Effects of **32h** on Hippo-YAP and Wnt pathways. (O) Effects of **32h** or RXDX-101 on Hippo-YAP and Wnt pathways in NTRK1-OE or HCT116 cells. (P) Induction of autophagy. (Q) LC3 Change, scale bar = 100 μm. (R) Cell viability. (S−T) LC3 expression (S) and cell viability (T) after addition of CQ (10 μmol/L) and Baf-A1 (50 nmol/L) for 1 h. (U) Cell colony formation. (V) Cell cycle. (W) Cell apoptosis. (X) Hoechst 33,258 staining. (Y) Bcl-2 and Bax expression. Data are mean ± SD, $n = 3$. NS, no significance, $*P < 0.05$, $**P < 0.01$, $***P < 0.001$ and $****P < 0.0001$.